Resveratrol protects photoreceptors by blocking caspase- and PARP-dependent cell death pathways

Shu-Yan Liu, Jing-Yao Song, Bin Fan, Ying Wang, Yi-Ran Pan, Lin Che, Ying-Jian Sun, Guang-Yu Li

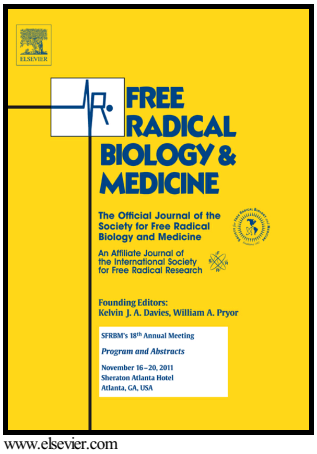

www.elsevier.com

PII: S0891-5849(18)31398-4
DOI: https://doi.org/10.1016/j.freeradbiomed.2018.10.431
Reference: FRB13995

To appear in: *Free Radical Biology and Medicine*

Received date: 14 August 2018
Revised date: 14 October 2018
Accepted date: 17 October 2018

Cite this article as: Shu-Yan Liu, Jing-Yao Song, Bin Fan, Ying Wang, Yi-Ran Pan, Lin Che, Ying-Jian Sun and Guang-Yu Li, Resveratrol protects photoreceptors by blocking caspase- and PARP-dependent cell death pathways, *Free Radical Biology and Medicine,* https://doi.org/10.1016/j.freeradbiomed.2018.10.431

Resveratrol protects photoreceptors by blocking caspase- and PARP-dependent cell death pathways

*Shu-Yan Liu[1], Jing-YaoSong[1], Bin Fan[1], Ying Wang[2], Yi-Ran Pan[1], Lin Che[1], Ying-Jian Sun[1], Guang-Yu Li[1]**

1 Department of Ophthalmology, Second Hospital of JiLin University, ChangChun 130041, China

2 Department of Hemooncolog, Second Hospital of JiLin University, ChangChun 130041, China

Correspondence to:

*Guang-Yu Li**

Department of Ophthalmology, Second Hospital of JiLin University, ChangChun 130041, China.

+81-431-89575858

Abstract

Retinal degeneration is a major cause of severe vision loss and irreversible blindness and is characterized by progressive damage to retinal photoreceptor cells. Resveratrol (RSV) serves as an activator of the histone deacetylase, Sirt1, and has been shown to exert anti-oxidative properties. In this study, we mimicked retinal degeneration by subjecting photoreceptors (661W cells) to glucose deprivation (GD) or light exposure. Under these conditions, we investigated the mechanisms underlying GD- or light exposure-induced cell death and the protective effect of RSV. We found that GD and light exposure resulted in mitochondrial dysfunction, oxidative stress, and cell death. Treatment of injured cells with RSV decreased the production of reactive oxygen species (ROS), improved the ratio of reduced/oxidized glutathione

(GSH/GSSG), mitochondrial membrane potential and morphology, and reduced apoptosis. We used the caspase inhibitor, z-VAD-fmk, and a lentiviral-mediated shRNA knockdown of PARP-1 to reveal that GD and light exposure-induced cell death have different underlying mechanisms; GD triggered a caspase-dependent cell death pathway, whereas light exposure triggered a PARP-dependent cell death pathway. The level of caspase-9 and caspase-3, upregulated following GD, were reduced by treatment with RSV. Similarly, the level of PARP-1 and AIF, upregulated following light exposure, were decreased by treatment with RSV. Additionally, treatment with RSV elevated the protein expression and enzymatic activity of Sirt1 and a Sirt1 inhibitor reduced the protective effect of RSV against insult-induced cellular injuries, indicating that RSV's protective effect may involve Sirt1 activation. Finally, we investigated the neuroprotection of RSV *in vivo*. Administration of RSV to mice under extreme light exposure led to a suppression of the light-induced thinning of the outer nuclear layer (ONL) detected by H&E staining and restored retinal function evaluated by electroretinography (ERG). Taken together, our findings provide evidence that treatment with RSV has neuroprotective effects on both GD and light exposure-induced cell death pathways in photoreceptor cells.

Introduction

Retinal degenerative diseases such as retinitis pigmentosa (RP) and age-related macular degeneration (AMD) are significant causes of visual impairment and irreversible blindness. The primary cause of retinal degeneration may be complex and involve a variety of hereditary and environmental factors. Although hundreds of causative gene mutations have been identified, the exact molecular pathways causing photoreceptor death are not yet fully understood. Light injury and retinal ischemia are considered major contributors to these diseases [1-4]. Anatomically, the photoreceptors are nestled closely to the choroidal vasculature and the choroid serves as the primary supplier of glucose, oxygen, and other metabolic nutrients required by photoreceptors [5]. Nonetheless, degeneration of the photoreceptors is associated with attenuation of the retinal arterioles. Glucose deprivation is, therefore, one of the major factors contributing to the pathological mechanism of retinal ischemia [6, 7]. Additionally, although photoreceptor cells sense the light (400–700nm) that initiates phototransduction and forms the retinal potential, prolonged or intense exposure to light causes cell death of photoreceptors, resulting in retinal degeneration and blindness[8].

Both these insults (light injury and GD) would independently increase cellular oxidative stress [9-12].The retina is particularly susceptible to oxidative stress due to its high level of oxygen consumption and its propensity to photosensitize[13].Oxidative damage normally triggers efficient cellular repair functions within a certain range. However, when the mitochondria-derived reactive

oxygen species (ROS) exceed the cellular antioxidant defense capacity, programmed cell death may be initiated.ROS can elicit heme release from hemoproteins[14]. The heme oxygenase (HO) family is composed of three isozymes: the inducible HO-1 and the constitutively-expressed HO-2 and HO-3[15, 16]. HO-1 is a ubiquitous and redox-sensitive inducible stress protein that can exert indirect, yet potent, anti-oxidative effects by degrading heme to carbon monoxide (CO), iron, and biliverdin[17].

Increasing evidence has suggested that photoreceptor cell death plays a key role in the pathogenesis of retinal degeneration [18, 19]. Apoptosis is the classical means of programmed cell death, activated either via the intrinsic (mitochondria-mediated) or extrinsic (death receptor-mediated) pathways. Activation of a cascade of proteolytic enzymes called caspases (cysteine-containing aspartate-specific proteases) is an important step in the apoptotic process, and caspase-3 is a common death executor for the both intrinsic and extrinsic apoptotic pathways[20].

Apart from apoptosis, there are an increasing number of caspase-independent pathways, such as parthanatos[21]. Parthanatos is a unique and highly choreographed form of cell death that occurs through the overactivation of the nuclear enzyme, PARP-1, also known as poly (ADP-ribose) synthetase 1 or poly (ADP-ribose) transferase 1[22].Parthanatos does not require caspases for its execution but is dependent on the PARP-1-mediated accumulation of PAR (poly ADP-ribose) and the subsequent nuclear translocation of the apoptosis-inducing factor (AIF)[23]. Ordinarily a beneficial mitochondrial protein, the nuclear translocation of AIF causes

large-scale DNA fragmentation and chromatin condensation, leading to cell death[24].

Resveratrol (RSV) is a polyphenolic compound that can be found in many plants such as the red grape, peanut, and mulberry. It was reported to exert various pharmacological benefits, with anti-oxidative, anti-aging, anti-inflammatory, and anti-carcinogenic uses, as well as neuronal and cardiovascular protection [25, 26]. An ever-growing body of *in vivo* and *in vitro* evidence points to the protective effects of RSV in various diseases [27-29]. RSV activates Sirt1 [30, 31], a member of a highly conserved gene family (sirtuins) encoding NAD+-dependent deacetylases, originally found to deacetylate histones leading to increased DNA stability and prolonged survival[32].Sirt1 is reportedly located in the mitochondria and participates in stress response pathways, apoptosis, inflammation, and metabolism[33-36].

So far, no clinical strategy has been issued to prevent retinal degeneration and restore visual function. Therefore, investigation into treatments that can block or even delay photoreceptor cell death are warranted. In the present study, we examined whether GD or light injury could induce different cell death pathways in photoreceptor cells and whether RSV's activation of Sirt1 could block this photoreceptor cell death.

Abbreviations

RSV	resveratrol
GD	glucose deprivation
ROS	reactive oxygen species
ONL	outer nuclear layer
ERG	electroretinography
RP	retinitis pigmentosa
AMD	age-related macular degeneration
HO	heme oxygenase
AIF	apoptosis-inducing factor
Sirt1	sirtuin 1

Materials and Methods

Drugs and inhibitors

Resveratrol (≥99%) was purchased from Sigma-Aldrich (Shanghai, China). z-VAD-fmk (> 95%) was purchased from Beyotime Biotechnology (Shanghai, China). Ex-527 (99.18%) was purchased from AbMole BioSciences (Houston, TX, USA).

Cell culture

The murine cone-photoreceptor cell line 661W was provided by Dr. Muayyad Al-Ubaidi (University of Oklahoma Health Sciences Center, Oklahoma, USA). Cell-culture media and all additives were purchased from HyClone Company (Beijing, China). The cells were maintained in Dulbecco's Modified Eagle Medium (DMEM) supplemented with 10% fetal bovine serum, 100 IU/mL streptomycin, and 100 IU/mL penicillin. The cells were incubated at 37°C in a humidified atmosphere of 95% air and 5% CO_2. Cells were trypsinized with 0.05% trypsin–EDTA and subsequently divided into culture plates as required.

In vitro RSV application, glucose deprivation, and light exposure

For the glucose deprivation experiment, approximately 90%-confluent 661W cells were cultured in 6-well or 96-well plates for 24 h with normal medium, washed two times with phosphate buffered saline (PBS), and then cultured in glucose-free medium for the maximum possible duration (until all the cells died).

For the light exposure experiment, approximately 70%-confluent 661W cells were cultured in 6-well or 96-well plates for 24 h with normal medium and then cultured in normal medium under light exposure (1500 lux) for the maximum possible duration

(until all the cells died).

RSV was dissolved in DMSO, diluted to different concentrations with double-distilled H_2O, and then applied at indicated concentrations until all cells in the control group died under GD or light exposure.

Lentiviral-mediated short hairpin RNA (shRNA) to establish a PARP knockdown cell line

For PARP-1 knockdown, a lentivirus expressing PARP-1-targeted short hairpin RNA (shRNA) was constructed by GeneCopoeia(Shanghai, China). Lentivirus expressing scrambled shRNA was used as a negative control (GeneCopoeia). The interfering sequence specific to the PARP-1 gene was as follows: Forward: 5'-TAATACGACTCACTATAGGG-3';

Reverse:5'-CTGGAATAGCTCAGAGGC-3'.The negative control sequence was as follows:

Forward:5'-TAATACGACTCACTATAGGG-3';Reverse:5'-CTGGAATAGCTCAGAGGC-3'.

The third-generation lentiviral package system (pRRE, pRSV-Rev, pCMV-VSVG) and target plasmid were used to package the lentiviral particles in human embryonic kidney 293T (HEK293T) cells. Lentiviral particles were concentrated 72 h post-transfection. In order to obtain a PARP-1 knockout cell line, the murine photoreceptor cell line 661W was then co-infected with virus particles. To avoid the viral toxicity, fresh DMEM completed media was added to replace the infection medium 24 h after adding the virus. To select stable cell lines, antibiotic-mediated

selection was started 2 d after transduction, using 6 μg/mL hygromycin (Sangon Biotech; Shanghai, China). After 2 weeks of treatment, stable colonies emerged while untransduced cells were killed after 48 h treatment with hygromycin.

Cell viability assay

Cell viability was assessed colorimetrically using 3-(4, 5-dimethylthiazolyl-2)-2, 5-diphenyltetrazolium bromide (MTT). The 661W cells were seeded in 96-well plates (1×10^4 cells/well) and incubated overnight. Then, the cells were treated with different concentrations of RSV for indicated time points under normal, GD, and light-exposure conditions. After treatment, cells in each well were incubated with 10 μL MTT (5 mg/mL in PBS, Sigma) at a final concentration of 500 μg/mL for 1 h at 37°C and the supernatant was removed. Next, 100 μL DMSO was added to each well and the plate was incubated at room temperature overnight. The absorbance was measured at 570 nm using a microplate reader (Tecan, Mannedorf, Swizerland). A dose-response curve was plotted and the IC50 value was calculated using GraphPad Prism 6 software.

Cell impedance assay

Cell impedance assays were performed using the xCELLigence RTCA instrument (ACEA Biosciences; San Diego, CA, USA). The impedance value of each well was automatically monitored by the xCELLigence system and expressed as a cell index (CI) value. Electronic impedance in the form of CI was derived corresponding to the relative density and adherence strength of cells in each well. Background measurements were taken from the wells by adding 50 μL of the same medium to the

E-plates-96.After calibration, 661W cells from an exponentially growing colony were seeded on a 16-well E-Plate at a density of 8,000 cells/well to a final volume of 150 μL. The E-plate Cardio 96 (ACEA Biosciences, San Diego, CA, USA) xCELLigence plate was inserted into the xCELLigence station that was kept in an incubator at 37°C with 5% CO_2.The cells were treated after equilibration. For the glucose deprivation experiment, the cells were washed twice with PBS and then cultured in glucose-free medium. For the light exposure experiment, cells were washed twice with PBS and then cultured in normal medium under light exposure. For the resveratrol experiments, RSV was applied at indicated concentrations during either GD or light exposure. The impedance signals were recorded every 5 min until the end of the experiment (up to 140 h).The raw data and statistical information were acquired using the RTCA 2.0 software (ACEA Biosciences, Inc., San Diego, CA, USA).

Propidium iodide (PI)**/Hoechst staining**

Based on the results of the cell impedance assay, the 661W cells were divided into the following five groups: DMEM only, GD or light exposure, administration of 10 μM RSV, 50 μM RSV, and 100 μM RSV. Cells were treated as described for 16 h of GD or 4 d of light exposure.

Cell death was characterized by double nuclear staining with Hoechst 33258 dye and propidium iodide (PI), both purchased from Beyotime Biotechnology (Shanghai, China). Cells were stained with the Hoechst dye (2 μg/mL) for 30 min at 37°C and consecutively stained with PI (5 μg/mL) and incubated in the dark for 10 min at 4°C. PI-positive cells were visualized under an inverted fluorescence microscope

(Olympus, Japan). The cell death percentage was calculated using the equation PI-positive cells/Hoechst-stained cells × 100.

Intracellular ROS measurement

Intracellular ROS was measured with an oxidation-sensitive fluorescence probe (DCFH-DA), purchased from Beyotime Biotechnology (Shanghai, China) and used exactly according to the manufacturer's instructions. Briefly, cells were washed twice with fresh medium after GD or light exposure and then incubated in 10 μM DCFH-DA at 37°C for 20 min. Oxidized 2,7-dichlorofluorescein (DCF) fluorescence was visualized under a fluorescence microscope (Olympus, Japan). Fluorescence intensity was measured at excitation and emission wavelengths of 488 nm and 525 nm, respectively. Fluorescence intensities were quantitatively analyzed using IP-Win32 software (NIH, Bethesda, MD).

Measurement of reduced/oxidized glutathione (GSH/GSSG)

The intracellular glutathione concentration was determined with a GSH and GSSG assay kit (Beyotime, Shanghai, China) according to the manufacturer's instructions. Briefly, after 16 h of GD or 4 d of light exposure, the media was removed, and cells were washed with PBS and harvested. The cells were mixed with 5% metaphosphoric acid and lysed with two cycles of freeze-thaw (freezing in liquid nitrogen and thawing at 37°C). The samples were then centrifuged at 10,000×*g* for 10 min at 4°C. The supernatant was collected to determine the levels of total glutathione and oxidized GSSG. The intracellular glutathione was determined by measuring the absorbance at 412 nm using a microplate reader (Tecan, Mannedorf, Swizerland).The reduced GSH

level was obtained by subtracting the level of GSSG from that of total glutathione.

Mitochondrial membrane potential assay

After 16 h of GD or 4 d of light exposure, medium was removed and cells were washed with Ca^{2+}/Mg^{2+}-free PBS. After incubation with the JC-1 staining solution (10 μg/mL; Beyotime Biotechnology, Shanghai, China) in a 37°C incubator for 30 min, cells were washed twice with JC-1 staining buffer and examined under a fluorescence microscope (Olympus, Japan) using 514 nm excitation and emissions at 529 nm and 590 nm. Fluorescence intensities were quantitatively analyzed using IP-Win32 software (NIH, Bethesda, MD).The percentage of JC-1-aggregated staining (red fluorescence) was calculated using the equation JC-1-aggregated cells/total cells × 100.

Confocal fluorescence imaging of MitoTracker Green

The distribution of mitochondria was labeled with MitoTracker Green (Beyotime, China).After 16 hours of GD or 4 d of light exposure, medium was removed and cells were washed twice with fresh pre-warmed PBS. They were then incubated in medium containing 100 nmol/L fluorescent mitochondrial probe at 37°C for 30 min. After two washes with PBS, the cells were subjected to confocal fluorescence imaging for mitochondrial measurements on the confocal laser scanning microscope (Olympus, Tokyo, Japan) using 490 nm excitation and emission at 516 nm.

Sirt1 activity assay

To quantify sirtuin 1 (Sirt1) activity, nuclear extracts were prepared from cells after 16 h of GD or 4 d of light exposure. Nuclear extracts were used to measure deacetylase

activity of an acetylated histone using the Epigenase Universal SIRT Activity/Inhibition Assay Kit (Epigentek, Farmingdale, NY, USA), according to the manufacturer's instructions. Briefly, 7.1 μg of nuclear extract was applied to microplate wells coated with an acetylated histone SIRT substrate. After incubation for 90 min, the SIRT-deacetylated products were recognized with a specific antibody. Finally, after adding antibody detection and color developing solution, the absorbance at 450 nm was measured with a microplate reader.

Animals

All animal experiments were conducted in accordance with the Association for Research in Vision and Ophthalmology Statement for the Use of Animals in Ophthalmic and Vision Research. Male BALB/c57 mice between 8 to 10 weeks of age were purchased from the Animal Center of Jilin University (Changchun, China) for use in the present study. The mice were housed in a temperature-controlled room at 21–23°C and kept on a 12 h, 2.5 lux light/dark cycle, with free access to food and water.

***In vivo* RSV treatment and light exposure protocol**

Mice were injected intraperitoneally with RSV at a dose of 22.4 mg/kg body wt per day for 7 consecutive days before the ERG. On the third day of RSV administration, the animals' pupils were dilated with atropine sulfate solution (SINQI, Shenyang, China). Then the mice were separated into individual boxes and exposed to bright continuous light for 12 h to induce retinal degeneration. The light source was a cool-white, 7000 lux, fluorescent tube light, measured using a portable lux meter.

After 12 h of light exposure, all mice were placed in the normal light/dark cycle for use prior to ERG measurement. After the ERG, the mice were euthanized with an overdose of sodium pentobarbital (Sigma-Aldrich Corp, Beijing, China) and the eyes were immediately enucleated for morphologic analysis. From each animal, one eye was allocated for histology studies, while the other was used for molecular studies of the retina.

Electroretinography (ERG)

Retinal function was evaluated using an electroretinogram (Metrovision, Perenchies, France).Dark-adapted (scotopic 0.01) and light-adapted (photopic 3.0ERG) ERGs were performed on all animals before the RSV injection to establish baseline standards. For the light exposure experimental group, the ERGs were obtained 5 d after light exposure. All mice were dark-adapted 2 h before ERG and all the preparations prior to recording were performed under dim red light. Mice were anesthetized via an intraperitoneal injection of sodium pentobarbital (60 mg/kg body wt), a dose sufficient to maintain effective anesthesia for 45 to 60 min. The pupils were dilated with a few drops of 1% tropicamide in saline (SINQI, Shenyang, China). Oxybuprocaine (Santen, Jiangsu, China) was applied topically for corneal anesthesia, and carbomer (BAUSCH&LOMB, Shandong, China) was applied for corneal hydration. The animals were placed on a heating pad that maintained their body temperature at 35–36°C throughout the experiment. The ground electrode was a needle inserted subcutaneously in the tail and the reference electrodes were placed subcutaneously in the lower jaw. The active recording electrodes were sliver wires

placed on the cornea. Once the setup under dim red light was complete, another 10 min of dark adaptation was allowed before commencement of recording. ERG analysis was based on amplitude measurements of the a- and b-waves.

Retinal histology and retinal thickness measurements

The retina was fixed with 4% paraformaldehyde overnight at room temperature, dehydrated with graded concentrations of ethanol in series, and then embedded in paraffin. Sagittal sections containing the whole retina were cut 3 μm thick for hematoxylin and eosin (H&E) staining. The outer nuclear layer (ONL) thickness was measured every 0.5 mm from the optic nerve head to the most peripheral region of the retina using the ImageJ program, and the average values were calculated.

Western blotting

For sample preparation from fresh retina, the retina was placed in 100 μL RIPA lysis buffer (Beyotime Biotechnology, Shanghai, China) and then sonicated. The lysate was centrifuged at 10 000 rpm for 15 min at 4°C. For sample preparation from 661W cells, the cells were collected and sonicated in RIPA lysate buffer. A bicinchoninic acid assay was used to estimate protein concentration. An equal amount (20 μg) of cell lysate was dissolved in sample buffer and samples were boiled for 5 min prior to gel loading. Electrophoresis was performed with 10% polyacrylamide gels containing 0.1% SDS. Proteins were transferred to nitrocellulose membranes, which were subsequently blocked with 5% non-fat dry milk in TBS-T (Tris-buffered saline with 0.1% Tween-20) for 1 h at room temperature. The membranes were then incubated for 3 h at room temperature with one of the following primary antibodies: anti-actin (1: 1000,

Signalway Technology, St. Louis, MO, USA), anti-HO-1 (1:1000, Bioworld Technology, Minneapolis, MN, USA), anti-Sirt1 rabbit polyclonal antibody (1:1000, Bioworld Technology, Minneapolis, MN, USA), anti-Caspase-3 (1:1000, Cell Signaling Technology, Beberly, MA, USA), anti-Caspase-9 (1:1000, Abcam, Cambridge, MA, USA), anti-PARP (1:1000, Cell Signaling Technology, Beberly, MA, USA), or anti-AIF (1: 3000, Santa Cruz, Dallas, TX, USA) diluted in TBS-T. The membranes were then washed three times in TBS-T and incubated with peroxidase-linked secondary antibodies diluted in TBS-T. Signals were developed using enhanced chemiluminescence and images were captured using a microscope equipped with a CCD camera (Tanon, Shanghai).Band density analysis of the proteins of interest was performed using Image J software and presented relative to the band density of the corresponding loading control.

Statistical Analysis

Statistical analyses were performed using SPSS v 24.0 (SPSS, Chicago, IL, USA). Each experiment was repeated at least three times. Data are expressed as means ± SEM. Differences between means were evaluated using one-way ANOVAs followed by post-hoc Bonferroni tests. $P < 0.05$ was considered statistically significant.

Results

3.1 Resveratrol protects 661W cells against GD- or light exposure-induced injuries

To determine the cellular injury resulting from the different insults (GD or light exposure) in 661W cells, we monitored cell viability and death rate under the GD or light-exposure conditions. First, we explored the hormetic effects of RSV using MTT cell viability assays under normal conditions (no insult). We observed that the hormetic zone of RSV emerged from 1 to 10 μM. Treatment with RSV increased the viability of 661W cells at these low concentrations but decreased cell viability at concentrations greater than 10 μM. The IC50 of RSV was **209.6** μM (Fig. 1A).

Next, we tested for biologically safe concentrations of RSV that were able to exert a protective effect against GD or light exposure-induced injury by exposing cells to a series of RSV concentrations (10 μM, 50 μM, 100 μM, 150 μM, 200 μM, and 300μM). The xCELLigence RTCA was used to analyze 661W cells in real-time. The mean impedance change (n = 2) was measured every 5 min and displayed as a cell index (CI) value. A high CI indicates more cell adhesion and vice versa, with a CI of zero signifying cell death. As shown in Figure 1, all the 661W cells died about 16 h after GD (Fig. 1B) or about 4 days after light exposure (Fig. 1C).Regardless of the type of insult used (GD or light exposure), RSV exhibited a protective effect at concentrations of 10 μM, 50 μM, and 100 μM, but showed a cytotoxic effect at concentrations of 150 μM, 200 μM, and 300 μM (Fig. 1 B and C). This result showed that doses below 100 uM are biologically safe concentrations of RSV. In cells under GD, 10 μM, 50 μM,

and 100 μM RSV offered immediate protection against cell death, within one hour after RSV treatment. For the first seven hours of GD, 10 μM RSV had the optimal protective effect, whereas in the last 9 hours of GD, 100 μM RSV offered the most protection from cell death (Fig. 1B). In the light exposure group, 10 μM, 50 μM, and 100 μM RSV played a protective role against cell death. Within 24 h after the start of light exposure, 10 μM RSV began to have a significant protective effect (Fig. 1C). By the second day after the start of light exposure, 100 μM RSV started to have a significant protective effect, which was maintained for more than 3 days.

To further confirm the protective effect of RSV, GD- or light-exposed cells were treated with biologically safe doses of RSV (10 μM, 50 μM, and 100 μM) and observed PI/Hoechst staining after 16 h of GD or 4 days of light exposure. As shown in Figure 1D and E, there was a higher rate of cell death at 16 h after GD or 4 days after light exposure compared to the control group, but RSV treatment significantly mitigated GD or light exposure-induced cell death. In the case of both GD and light exposure-induced injuries, the amount of cell death was significantly reduced with increasing concentrations of RSV (Fig. 1F and G; $P < 0.01$). These results suggest that RSV protects 661W cells against GD or light exposure-induced injuries, with the 100 μM dose being the optimum protective concentration.

3.2 Resveratrol attenuated GD- or light exposure-induced intracellular ROS generation and improved oxidative status

Both GD and light exposure induced massive production of intracellular ROS in 661W cells. The level of intracellular ROS was measured using a DCFH-DA probe.

As shown in Figure 2A and B, both insults (GD and light exposure) markedly increased ROS production (green fluorescence) compared to the control group, while the RSV-treated groups showed significantly attenuated cellular ROS generation. The protective effect of RSV was dose-dependent; the higher the concentration of RSV, the lower the intracellular ROS production (Fig. 2C and D; $P < 0.01$).

Reduced glutathione (GSH) is one of the most important scavengers of ROS, and its ratio with oxidized glutathione (GSSG) has been regarded as a marker of oxidative stress. As shown in Fig. 2E, we determined cellular GSH/GSSG ratios and found that cells under GD and light exposure had a lower GSH/GSSG ratio than control cells. However, treatment with RSV potently reversed the decrease in GSH/GSSG caused by GD and light exposure.

The inducible and redox-regulated enzyme, HO-1 is considered to have an important role in the oxidative stress response of the cell. We measured the expression of HO-1 in glucose-deprived and light exposed cells by western blot (Fig. 2F).Both insults (GD and light exposure) markedly upregulated HO-1 expression compared to the control group. Moreover, treatment with 100 μM RSV further enhanced the insult-induced upregulation of HO-1 when compared to the vehicle group ($P < 0.01$) (Figure 2G and H). Taken together, these results suggest that cells undergo severe oxidative stress during the course of GD or light exposure and RSV effectively ameliorates this by suppressing intracellular ROS generation, increasing reduced glutathione levels, and augmenting the level of the stress-response protein HO-1.

3.3 Resveratrol maintains mitochondrial function

Mitochondria are involved in diverse processes including energy and redox homeostasis. To assess mitochondrial function, we investigated mitochondrial morphology and the mitochondrial membrane potential ($\Delta\psi m$).As shown in Figure 3A,mitochondria exposed to either GD or light exposure showed more prominent morphological alterations; compared to the elongated, filamentous mitochondria in the control group, the cells exposed to insults exhibited more oval and round mitochondria. However, treatment with 100 μM RSV significantly ameliorated the morphological defect of mitochondria.We used the JC-1 staining reagent to assess $\Delta\psi m$; JC-1 gets incorporated at low concentrations in depolarized mitochondria and fluoresces green but it aggregates at high concentrations in hyperpolarized mitochondria and fluoresces in the yellow/red range. Accordingly, Figure 3B and C showed that the mitochondria under either GD or light exposure were depolarized (green fluorescence) compared to those of control cells (yellow to red fluorescence). However, treatment with RSV significantly attenuated changes in $\Delta\psi m$, as indicated by increased red fluorescence (Fig. 3B and C) and the percentage of JC-1-aggregated cells (Fig. 3D and E) when compared to the vehicle group ($P < 0.01$). Similar to the other protective effects of RSV, the number of JC-1-aggregated cells were also significantly concentration-dependent ($P < 0.01$).These results suggest that RSV can effectively maintain mitochondrial function after either GD or light exposure.

3.4 Resveratrol protects 661W cells by activating Sirt-1

To determine whether the protective effect of RSV is mediated by its activation of Sirt1, we employed the Sirt1 inhibitor, Ex-527. As shown in Figure 4A–D, there is a

lower cell death rate in the presence of RSV in both the GD and the light exposure groups compared to the control group, whereas treatment with Ex-527 reversed this trend ($P < 0.01$). Next, we examined the total protein expression of Sirt1 by western blot (Fig. 4E). As quantified in Figure 4F and G, Sirt1 expression level was significantly increased in both GD and light exposure groups ($P < 0.01$). Application of 100 μM RSV in either glucose deprived or light exposed cells further enhanced the Sirt1 protein expression ($P < 0.01$). To determine whether Sirt1 enzymatic activity was indeed elevated by the insults, we prepared nuclear extracts from cells in both the GD and light exposure groups and confirmed that the deacetylation activity of Sirt1 was accelerated under these conditions (Fig. 4H). RSV-induced Sirt1 upregulation was also confirmed by this Sirt1 activity assay (Fig. 4H). Collectively, these results suggest that RSV protects cells from insult-induced death by activating Sirt1.

3.5 Resveratrol blocks GD or light-induced cell death via different pathways

Mitochondria are the instigators and center of apoptosis. The activation of mitochondria-mediated signaling pathways induces cell apoptosis. The classical caspase-dependent signaling pathway plays an important role in the apoptosis process. To evaluate the role of caspases in either GD or light exposure-induced cell death, we blocked caspase activation with a non-specific caspase inhibitor (z-VAD-fmk). Figure 5A shows a marked decrease in the number of cells that stained positive for PI compared to the GD group ($P < 0.01$), indicating significantly reduced GD-induced cell death after z-VAD-fmk application, while light exposure-induced cell death remained unchanged even in the presence of the inhibitor. Next, we studied the

protein expression of the specific proteins, caspase-3, and caspase-9, by western blot (Fig. 5C). As quantified in Figure 5D, while GD markedly upregulated the levels of both caspase-3 and caspase-9 compared to the control group ($P < 0.01$), treatment with 100 μM RSV remarkably reduced expression of both these critical caspases ($P < 0.01$). Under light exposure, however, protein expression of caspase-3 and caspase-9 did not change a significant amount with and without RSV (Fig. 5E). These results suggest that RSV inhibits GD-induced cell death by inhibiting the caspase-dependent pathway, whereas the caspase-dependent pathway has a negligible role in light exposure-induced cell death.

Having ruled out a caspase-mediated mechanism for light exposure-induced cell death, we next investigated whether parthanatos, a caspase-independent mechanism of apoptosis, was involved. To evaluate the role of this PARP-1-dependent pathway in light exposure-induced cell death, we used a lentiviral-mediated shRNA approach to knock down PARP-1 expression in 661W cells and then stained with PI/Hoechst to quantify cell death. As demonstrated by the low number of PI-positive cells in the shRNA group (Figure 6A), PARP-1 knockdown significantly decreased light exposure-induced cell apoptosis ($P < 0.01$). We also measured the protein expression of PARP-1 and AIF with western blotting. We observed a cleaved form of PARP-1in the GD group, as PARP-1 is a substrate of caspase-3 ($P < 0.01$) (Fig. 6D). However, full-length PARP-1 and active form of AIF were significantly upregulated in the light exposure group when compared to the control group ($P < 0.01$) (Fig. 6E and F). Treatment with 100 μM RSV significantly reversed these trends ($P < 0.01$). These

results suggest that RSV inhibits light exposure-induced cell death by inhibiting members of the PARP-dependent cell death pathway.

3.6 Resveratrol inhibits light exposure-induced retinal dysfunction and ONL thinning *in vivo*

To investigate the effect of RSV on retinal dysfunction *in vivo*, we exposed naïve or RSV-treated mice to continuous bright light for 12 h and performed ERG analysis. As shown in Figure 7A–D, naïve mice that underwent extreme light exposure exhibited a marked decrease in the amplitude of scotopic a- and photopic b-waves compared to control group mice receiving no light exposure ($P < 0.01$). A 7-day course of RSV to light-exposed mice significantly restored the amplitude reduction of a-waves and b-waves compared to vehicle-treated mice ($P < 0.01$). These results provide evidence supporting a neuroprotective role of RSV *in vivo* and can suppress light exposure-induced retinal dysfunction. To further evaluate the effect of RSV on light-induced histological damage to the retina, the outer nuclear layer (ONL) thickness was analyzed by H&E staining (Fig. 7E). As quantified in Figure 7F, extreme light exposure led to a significant reduction in ONL thickness compared to control mice receiving no extreme light exposure ($P < 0.01$). Intraperitoneal injections of RSV to light-exposed mice significantly suppressed the thinning of the ONL compared to the untreated, light-exposed group. To reconfirm *in vivo* that parthanatos is involved in the light exposure-induced photoreceptor apoptosis, we measured the retinal expression of AIF and PARP-1 with western blot from mice exposed to extreme light (Fig. 7G). As shown in Figure 7H, the retinal expression of AIF and

PARP-1 was increased in light-exposed mice when compared to the control group ($P < 0.01$). However, treatment with RSV significantly reversed these trends. These results suggest that treatment with RSV effectively protects against retinal thinning and inhibits light exposure-induced photoreceptor cell death by inhibiting the PARP-dependent cell death pathway.

Discussion

In this study, we showed that RSV activates Sirt1 to effectively protect either GD or light exposure-induced photoreceptor cell death via different pathways. During retinal degeneration, retinal cells undergo various pathophysiological changes. Photoreceptor cell death is usually recognized as the essential feature shared by human disease models of retinal degeneration[37, 38].We employed real-time cell analysis (RTCA) to assess photoreceptor cell death in real-time. RTCA uses microelectrodes to detect impedance changes proportional to the number of adherent cells and expresses this measure as the cell index (CI). Our results demonstrated that 661W cells were all dead after about 16 h of GD, characterized by acute energy failure. However, the light exposure-induced cell death was relatively mild and slow compared to the effect of the GD insult, with cells beginning to die 2–3 days after the start of the insult and all cells dying after about 4 days of light exposure. To corroborate the real-time data, we also used PI/Hoechst staining to determine the cell death ratio under either GD or light exposure. Normally, apoptotic cells are characterized by DNA fragmentation and, consequently, loss of nuclear DNA content. Therefore, a fluorescent, membrane-impermeable molecule like PI is excluded from viable cells and incorporated into apoptotic cells. Its ability to bind and label DNA makes it possible to obtain a rapid and precise evaluation of apoptosis simply by counting PI-positive cells. Although RTCA and PI staining use different methods to evaluate dead cells under GD and light exposure conditions, we observed consistent results from both these techniques.

Cell death is usually the result of an imbalance between pro-oxidant and anti-oxidant factors in cells, caused by severe oxidative stress[39]. We used a fluorescent probe to measure intracellular ROS as a proxy for oxidative stress. ROS has been verified to play a pivotal role in the initiation of cell death pathways. Our results demonstrated that while 661W cells exhibited weak green fluorescence in the control group, enhanced green fluorescence was observed 16 h after GD or 4 days after light exposure, implying that both these insults caused severe oxidative stress in the cells.

In order to maintain redox homeostasis when subjected to oxidative stress, cells activate a pro-survival pathway mediated by protective genes called vitagenes. Vitagenes encode sirtuins, thioredoxin, heme oxygenase-1 (HO-1), and heat shock proteins (HSPs), which together contribute to establishing a cytoprotective state in a wide variety of human diseases [40]. Calabrese and colleagues found that vitagene upregulation promoted resilience in damaged neurons and hence improved cellular resistance against proteotoxic insults and apoptotic neurodegeneration[41].

RSV is a polyphenolic phytoalexin with hormetic effects at low doses that provide widespread benefits to systemic health. In a clinical study, Richer and colleagues observed that the daily oral consumption of a low dose of Longevinex® (an RSV-containing, non-prescription drug) restored retinal structure and visual function in octogenarians[42]. RSV was also shown to mitigate the symptoms of a variety of ophthalmic diseases including diabetic retinopathy, glaucoma, and macular degeneration[43-45]. RSV is a natural compound with anti-oxidative and

anti-inflammatory properties. In fact, oxidative-stress markers have been observed in the brains of patients with neurodegenerative diseases, which support the rationale for neuroprotective nutritional interventions based on the action of antioxidants and anti-inflammatory agents. Interestingly, Sauer and colleagues demonstrated that non-toxic concentrations of RSV promoted the production of oxidation products such as ROS. In contrast to the common perception that RSV acts mainly as an antioxidant, they proposed that the cellular response to RSV treatment is essentially based on oxidative triggering[46]. Notably, RSV is a known activator of the vitagene-encoded histone deacetylase, Sirt1, which plays a protective role against oxidative injury in several neurodegenerative diseases. Sirt1 is a member of the sirtuin family. It is mainly a nuclear enzyme but can also be found in mitochondria. The expression of Sirt1 is known to be controlled at both the transcriptional and post-transcriptional levels. Han and colleagues demonstrated that HDAC4 increased Sirt1 sumoylation, thereby stabilizing its protein levels to delay cellular senescence[47]. Sirt1 has also been shown to protect the cell from apoptosis induced by oxidative stress[48]. Our study found that administration of a Sirt1 inhibitor markedly inhibited the protective effect of RSV on 661W cells under either GD or light exposure. Treatment with RSV enhanced Sirt1 protein expression. This activation may function as an upstream signal in the death cascade and is a critical point in averting GD- or light exposure-induced death of photoreceptors.

However, the mechanisms underlying GD and light exposure-induced oxidative stress are different. Evidence from earlier studies of GD-induced oxidative stress

suggests that the nicotinamide adenine dinucleotide phosphate (NADPH) oxidase (Nox) family of enzymes is an important generator of ROS. All Nox enzymes are known to generate ROS through the transfer of electrons from NADPH via intermediates to oxygen [49, 50]. Light exposure in the visible and UV range can induce photochemical lesions in retinal tissue, with particular susceptibility to wavelengths within the blue region of the spectrum. Lipofuscin is a byproduct of the phagocytosis of outer segments of lipid-rich photoreceptors and has been regarded as the mediator of blue light damage[51]. Studies have demonstrated that lipofuscin is a potent photo inducible generator of ROS and that it is phototoxic to retinal cells [52, 53].

The cellular response to oxidative stress, regardless of the causative mechanism, is often mediated by the upregulation of endogenous antioxidant defense components including HO-1[54]. HO-1 is induced by its substrate heme, as well as by various oxidative stresses, and is thought to play an important protective role against oxidative injuries. Calabrese and colleagues reported higher levels of the vitagenes Heat Shock Protein 72 (Hsp72) and HO-1 in the blood of patients with glaucoma compared with the levels in control individuals. These changes were associated with the increased expression of Trx and Sirt1 in the same experimental group[55]. In line with this, we found that both GD and light exposure increased the expression of the stress-response proteins HO-1 and Sirt1.

Mitochondria are both targets and important sources of ROS. These organelles serve as regulatory centers of the cell and are one of the most sensitive to various

injuries. Although a certain level of oxidative stress promotes mitochondrial growth, more severe stress can trigger mitochondrial dysfunction and cell death. Accordingly, we observed alterations in the morphology and the membrane potential of glucose-deprived or light-exposed mitochondria that were clear signs of mitochondrial dysfunction. Mitochondria are known to have a central role in the induction of apoptotic cell death by releasing various apoptotic factors such as cytochrome C, Smac/Diablo, HtrA2, Endo G, and AIF, which interact with cytosolic factors to trigger both caspase-dependent and caspase-independent cell death. Interestingly, we revealed that GD- and light exposure-induced cell death pathways were mediated by different mitochondrial signaling pathways. GD induced a caspase-dependent pathway involving specifically caspase-3 and caspase-9, whereas light exposure induced a caspase-independent pathway involving AIF and PARP-1.

Although caspases are thought to be central elements in the apoptotic program, recent data indicates that apoptosis may also be mediated by a caspase-independent mechanism called parthanatos that involves pro-apoptotic mitochondrial factors like AIF and PARP. Our data showed that treatment with a caspase inhibitor did not prevent light exposure-induced cell death. This indicates that, unlike GD, the light exposure insult triggers an apoptosis pathway independent of caspases. Previous studies have reported that when DNA damage is profound, the excessive activation of PARP-1 causes dissipation of the mitochondrial membrane potential and translocation of AIF from the mitochondria to the nucleus, leading to caspase-independent cell death.AIF can also induce purified mitochondria to release cytochrome c and

caspase-9, suggesting that AIF, once released from mitochondria, accelerates membrane permeabilization in a positive feedforward loop [56, 57]. We used an shRNA knockdown of PARP-1 in the 661W photoreceptor-derived cell line and PI/Hoechst staining to determine the cell death under light exposure. Our results demonstrated that PARP-1 knockdown cells exhibited significantly decreased cell death as compared to control, suggesting that PARP-1 function was critical to photoreceptor survival in the context of light exposure. We confirmed that treatment with RSV significantly suppressed the light exposure-induced the levels of PARP-1 and AIF protein expression, which provided further evidence to support that RSV inhibits light exposure-induced cell death by inhibiting the PARP-dependent pathway. AIF is a much larger protein than cytochrome c, and would hence take a longer time to translocate to the nucleus. This further explains why GD-induced, rapid cell death is a caspase-dependent pathway and light exposure-induced, relatively chronic cell death is a PARP-dependent pathway.

We enhanced the applicability of this study by testing RSV's protective effect on retinal dysfunction *in vivo*. Photoreceptor loss is a critical event during light exposure-induced retinal degeneration[58]. The ONL, composed exclusively of photoreceptor cell bodies, is a known target of light-induced retinal degeneration[59]. In accordance with the data on apoptotic cell death, we observed that treatment with RSV to light-exposed mice resulted in significant suppression of ONL thinning. The level of retinal PARP and AIF protein expression reconfirmed that light exposure-induced photoreceptor cell death is PARP-dependent pathway. To confirm

these histological data, we analyzed retinal function using ERG i*n vivo*. Light exposure is known to cause damage to retinal function represented by ERG. Light exposure-induced suppression of both a-waves and b-waves in the ERG was reversed by treatment with RSV. This was consistent with its effects on the histological changes in the photoreceptor cells, suggesting that the amelioration of retinal dysfunction is attributed to RSV-mediated suppression of ONL injury. The *in vivo* data clearly highlight the neuroprotective effects of RSV on retinal degeneration.

In summary, our study identified the protective effects of RSV on either GD or light-induced photoreceptor cell death. A schematic of this protective effect is depicted in Figure 8. RSV can effectively reduce cell death by activating Sirt1, which may function as an upstream signal in the death cascade. We found that RSV inhibits GD-induced cell death by inhibiting the caspase-dependent pathway and inhibits light injury-induced cell death by inhibiting the PARP-dependent pathway. We also demonstrated that RSV significantly protected against ONL thinning and restored retinal function. Unlike many other drugs, RSV is a naturally occurring, beneficial compound found in the human diet. In addition to this significant advantage, the findings from our study provide strong evidence for the treatment of retinal degeneration with RSV.

Acknowledgments

The authors thank Dr. Muayyad Al-Ubaidi (Department of Cell Biology, University of Oklahoma Health Sciences Center, Oklahoma City, OK) for generously providing the 661W cell line. This work was supported by the National Natural Science Foundation of China (No. 81570864) and the Natural Science Foundation of Jilin Province (No. 20160101004JC; No. 20160414045GH).

Conflicts of Interest

No author has a proprietary interest or a conflict of interest related to this submission.

References

[1] Zhu, Y. X.; Yao, J.; Liu, C.; Hu, H. T.; Li, X. M.; Ge, H. M.; Zhou, Y. F.; Shan, K.; Jiang, Q.; Yan, B. Long non-coding RNA MEG3 silencing protects against light-induced retinal degeneration. *Biochem Biophys Res Commun* **496:**1236-1242; 2018.

[2] Behar-Cohen, F.; Martinsons, C.; Vienot, F.; Zissis, G.; Barlier-Salsi, A.; Cesarini, J. P.; Enouf, O.; Garcia, M.; Picaud, S.; Attia, D. Light-emitting diodes (LED) for domestic lighting: any risks for the eye? *Prog Retin Eye Res* **30:**239-257; 2011.

[3] Miller, J. W.; Le Couter, J.; Strauss, E. C.; Ferrara, N. Vascular endothelial growth factor a in intraocular vascular disease. *Ophthalmology* **120:**106-114; 2013.

[4] Renner, M.; Stute, G.; Alzureiqi, M.; Reinhard, J.; Wiemann, S.; Schmid, H.; Faissner, A.; Dick, H. B.; Joachim, S. C. Optic Nerve Degeneration after Retinal Ischemia/Reperfusion in a Rodent Model. *Front Cell Neurosci* **11:**254; 2017.

[5] Berkowitz, B. A.; Schmidt, T.; Podolsky, R. H.; Roberts, R. Melanopsin Phototransduction Contributes to Light-Evoked Choroidal Expansion and Rod L-Type Calcium Channel Function In Vivo. *Invest Ophthalmol Vis Sci* **57:**5314-5319; 2016.

[6] Osborne, N. N.; Casson, R. J.; Wood, J. P.; Chidlow, G.; Graham, M.; Melena, J. Retinal ischemia: mechanisms of damage and potential therapeutic strategies. *Prog Retin Eye Res* **23:**91-147; 2004.

[7] Fan, B.; Wang, B. F.; Che, L.; Sun, Y. J.; Liu, S. Y.; Li, G. Y. Blockage of NOX2/MAPK/NF-kappaB Pathway Protects Photoreceptors against Glucose Deprivation-Induced Cell Death. *Oxid Med Cell Longev* **2017:**5093473; 2017.

[8] Contin, M. A.; Benedetto, M. M.; Quinteros-Quintana, M. L.; Guido, M. E. Light pollution: the possible consequences of excessive illumination on retina. *Eye (Lond)* **30:**255-263; 2016.

[9] Organisciak, D. T.; Vaughan, D. K. Retinal light damage: mechanisms and protection. *Prog Retin Eye Res* **29:**113-134; 2010.

[10] Kapupara, K.; Wen, Y. T.; Tsai, R. K.; Huang, S. P. Soluble P-selectin promotes retinal ganglion cell survival through activation of Nrf2 signaling after ischemia injury. *Cell Death Dis* **8:**e3172; 2017.

[11] Rivera, J. C.; Dabouz, R.; Noueihed, B.; Omri, S.; Tahiri, H.; Chemtob, S. Ischemic Retinopathies: Oxidative Stress and Inflammation. *Oxid Med Cell Longev* **2017:**3940241; 2017.

[12] Marie, M.; Bigot, K.; Angebault, C.; Barrau, C.; Gondouin, P.; Pagan, D.; Fouquet, S.; Villette, T.; Sahel, J. A.; Lenaers, G.; Picaud, S. Light action spectrum on oxidative stress and mitochondrial damage in A2E-loaded retinal pigment epithelium cells. *Cell Death Dis* **9:**287; 2018.

[13] Beatty, S.; Koh, H.; Phil, M.; Henson, D.; Boulton, M. The role of oxidative stress in the pathogenesis of age-related macular degeneration. *Surv Ophthalmol* **45:**115-134; 2000.

[14] Gozzelino, R.; Jeney, V.; Soares, M. P. Mechanisms of cell protection by heme oxygenase-1. *Annu Rev Pharmacol Toxicol* **50:**323-354; 2010.

[15] Cruse, I.; Maines, M. D. Evidence suggesting that the two forms of heme oxygenase are products of different genes. *J Biol Chem* **263:**3348-3353; 1988.

[16] McCoubrey, W. K., Jr.; Huang, T. J.; Maines, M. D. Isolation and characterization of a cDNA from the rat brain that encodes hemoprotein heme oxygenase-3. *Eur J Biochem* **247:**725-732; 1997.

[17] Motterlini, R.; Green, C. J.; Foresti, R. Regulation of heme oxygenase-1 by redox signals involving nitric oxide. *Antioxid Redox Signal* **4:**615-624; 2002.

[18] Reme, C. E.; Grimm, C.; Hafezi, F.; Marti, A.; Wenzel, A. Apoptotic cell death in retinal degenerations. *Prog Retin Eye Res* **17:**443-464; 1998.

[19] Grimm, C.; Wenzel, A.; Groszer, M.; Mayser, H.; Seeliger, M.; Samardzija, M.; Bauer, C.; Gassmann,

M.; Reme, C. E. HIF-1-induced erythropoietin in the hypoxic retina protects against light-induced retinal degeneration. *Nat Med* **8:**718-724; 2002.

[20] Elmore, S. Apoptosis: a review of programmed cell death. *Toxicol Pathol* **35:**495-516; 2007.

[21] Fatokun, A. A.; Dawson, V. L.; Dawson, T. M. Parthanatos: mitochondrial-linked mechanisms and therapeutic opportunities. *Br J Pharmacol* **171:**2000-2016; 2014.

[22] Andrabi, S. A.; Dawson, T. M.; Dawson, V. L. Mitochondrial and nuclear cross talk in cell death: parthanatos. *Ann N Y Acad Sci* **1147:**233-241; 2008.

[23] David, K. K.; Andrabi, S. A.; Dawson, T. M.; Dawson, V. L. Parthanatos, a messenger of death. *Front Biosci (Landmark Ed)* **14:**1116-1128; 2009.

[24] Wang, Y.; Dawson, V. L.; Dawson, T. M. Poly(ADP-ribose) signals to mitochondrial AIF: a key event in parthanatos. *Exp Neurol* **218:**193-202; 2009.

[25] Li, C.; Wang, L.; Huang, K.; Zheng, L. Endoplasmic reticulum stress in retinal vascular degeneration: protective role of resveratrol. *Invest Ophthalmol Vis Sci* **53:**3241-3249; 2012.

[26] Kubota, S.; Kurihara, T.; Mochimaru, H.; Satofuka, S.; Noda, K.; Ozawa, Y.; Oike, Y.; Ishida, S.; Tsubota, K. Prevention of ocular inflammation in endotoxin-induced uveitis with resveratrol by inhibiting oxidative damage and nuclear factor-kappaB activation. *Invest Ophthalmol Vis Sci* **50:**3512-3519; 2009.

[27] Kumar, S.; Eroglu, E.; Stokes, J. A., 3rd; Scissum-Gunn, K.; Saldanha, S. N.; Singh, U. P.; Manne, U.; Ponnazhagan, S.; Mishra, M. K. Resveratrol induces mitochondria-mediated, caspase-independent apoptosis in murine prostate cancer cells. *Oncotarget* **8:**20895-20908; 2017.

[28] Zhang, W.; Wang, X.; Chen, T. Resveratrol induces mitochondria-mediated AIF and to a lesser extent caspase-9-dependent apoptosis in human lung adenocarcinoma ASTC-a-1 cells. *Mol Cell Biochem* **354:**29-37; 2011.

[29] Lindsey, J. D.; Duong-Polk, K. X.; Hammond, D.; Leung, C. K.; Weinreb, R. N. Protection of injured retinal ganglion cell dendrites and unfolded protein response resolution after long-term dietary resveratrol. *Neurobiol Aging* **36:**1969-1981; 2015.

[30] Zhang, H.; He, S.; Spee, C.; Ishikawa, K.; Hinton, D. R. SIRT1 mediated inhibition of VEGF/VEGFR2 signaling by Resveratrol and its relevance to choroidal neovascularization. *Cytokine* **76:**549-552; 2015.

[31] Khan, R. S.; Fonseca-Kelly, Z.; Callinan, C.; Zuo, L.; Sachdeva, M. M.; Shindler, K. S. SIRT1 activating compounds reduce oxidative stress and prevent cell death in neuronal cells. *Front Cell Neurosci* **6:**63; 2012.

[32] Michan, S.; Sinclair, D. Sirtuins in mammals: insights into their biological function. *Biochem J* **404:**1-13; 2007.

[33] Yang, L.; Duan, Z.; Liu, X.; Yuan, Y. N-acetyl-l-cysteine ameliorates the PM2.5-induced oxidative stress by regulating SIRT-1 in rats. *Environ Toxicol Pharmacol* **57:**70-75; 2018.

[34] Pant, K.; Yadav, A. K.; Gupta, P.; Islam, R.; Saraya, A.; Venugopal, S. K. Butyrate induces ROS-mediated apoptosis by modulating miR-22/SIRT-1 pathway in hepatic cancer cells. *Redox Biol* **12:**340-349; 2017.

[35] Mendes, K. L.; Lelis, D. F.; Santos, S. H. S. Nuclear sirtuins and inflammatory signaling pathways. *Cytokine Growth Factor Rev* **38:**98-105; 2017.

[36] Karandrea, S.; Yin, H.; Liang, X.; Slitt, A. L.; Heart, E. A. Thymoquinone ameliorates diabetic phenotype in Diet-Induced Obesity mice via activation of SIRT-1-dependent pathways. *PLoS One* **12:**e0185374; 2017.

[37] Sweigard, J. H.; Matsumoto, H.; Smith, K. E.; Kim, L. A.; Paschalis, E. I.; Okonuki, Y.; Castillejos, A.;

Kataoka, K.; Hasegawa, E.; Yanai, R.; Husain, D.; Lambris, J. D.; Vavvas, D.; Miller, J. W.; Connor, K. M. Inhibition of the alternative complement pathway preserves photoreceptors after retinal injury. *Sci Transl Med* **7:**297ra116; 2015.

[38] Szczesny, P. [Morphologic changes in photoreceptor connecting cilia in experimental phototoxic retinopathy]. *Klin Oczna* **104:**195-200; 2002.

[39] Uttara, B.; Singh, A. V.; Zamboni, P.; Mahajan, R. T. Oxidative stress and neurodegenerative diseases: a review of upstream and downstream antioxidant therapeutic options. *Curr Neuropharmacol* **7:**65-74; 2009.

[40] Calabrese, V.; Cornelius, C.; Dinkova-Kostova, A. T.; Calabrese, E. J.; Mattson, M. P. Cellular stress responses, the hormesis paradigm, and vitagenes: novel targets for therapeutic intervention in neurodegenerative disorders. *Antioxid Redox Signal* **13:**1763-1811; 2010.

[41] Trovato Salinaro, A.; Pennisi, M.; Di Paola, R.; Scuto, M.; Crupi, R.; Cambria, M. T.; Ontario, M. L.; Tomasello, M.; Uva, M.; Maiolino, L.; Calabrese, E. J.; Cuzzocrea, S.; Calabrese, V. Neuroinflammation and neurohormesis in the pathogenesis of Alzheimer's disease and Alzheimer-linked pathologies: modulation by nutritional mushrooms. *Immun Ageing* **15:**8; 2018.

[42] Richer, S.; Stiles, W.; Ulanski, L.; Carroll, D.; Podella, C. Observation of human retinal remodeling in octogenarians with a resveratrol based nutritional supplement. *Nutrients* **5:**1989-2005; 2013.

[43] Soufi, F. G.; Mohammad-Nejad, D.; Ahmadieh, H. Resveratrol improves diabetic retinopathy possibly through oxidative stress - nuclear factor kappaB - apoptosis pathway. *Pharmacol Rep* **64:**1505-1514; 2012.

[44] Pirhan, D.; Yuksel, N.; Emre, E.; Cengiz, A.; Kursat Yildiz, D. Riluzole- and Resveratrol-Induced Delay of Retinal Ganglion Cell Death in an Experimental Model of Glaucoma. *Curr Eye Res* **41:**59-69; 2016.

[45] Nagineni, C. N.; Raju, R.; Nagineni, K. K.; Kommineni, V. K.; Cherukuri, A.; Kutty, R. K.; Hooks, J. J.; Detrick, B. Resveratrol Suppresses Expression of VEGF by Human Retinal Pigment Epithelial Cells: Potential Nutraceutical for Age-related Macular Degeneration. *Aging Dis* **5:**88-100; 2014.

[46] Plauth, A.; Geikowski, A.; Cichon, S.; Wowro, S. J.; Liedgens, L.; Rousseau, M.; Weidner, C.; Fuhr, L.; Kliem, M.; Jenkins, G.; Lotito, S.; Wainwright, L. J.; Sauer, S. Hormetic shifting of redox environment by pro-oxidative resveratrol protects cells against stress. *Free Radic Biol Med* **99:**608-622; 2016.

[47] Han, X.; Niu, J.; Zhao, Y.; Kong, Q.; Tong, T.; Han, L. HDAC4 stabilizes SIRT1 via sumoylation SIRT1 to delay cellular senescence. *Clin Exp Pharmacol Physiol* **43:**41-46; 2016.

[48] Hasegawa, K.; Wakino, S.; Yoshioka, K.; Tatematsu, S.; Hara, Y.; Minakuchi, H.; Washida, N.; Tokuyama, H.; Hayashi, K.; Itoh, H. Sirt1 protects against oxidative stress-induced renal tubular cell apoptosis by the bidirectional regulation of catalase expression. *Biochem Biophys Res Commun* **372:**51-56; 2008.

[49] Bhatt, L.; Groeger, G.; McDermott, K.; Cotter, T. G. Rod and cone photoreceptor cells produce ROS in response to stress in a live retinal explant system. *Mol Vis* **16:**283-293; 2010.

[50] Kowluru, A.; Kowluru, R. A. Phagocyte-like NADPH oxidase [Nox2] in cellular dysfunction in models of glucolipotoxicity and diabetes. *Biochem Pharmacol* **88:**275-283; 2014.

[51] Boulton, M.; Rozanowska, M.; Rozanowski, B.; Wess, T. The photoreactivity of ocular lipofuscin. *Photochem Photobiol Sci* **3:**759-764; 2004.

[52] Chen, W. J.; Wu, C.; Xu, Z.; Kuse, Y.; Hara, H.; Duh, E. J. Nrf2 protects photoreceptor cells from photo-oxidative stress induced by blue light. *Exp Eye Res* **154:**151-158; 2017.

[53] Zhao, Z.; Sun, T.; Jiang, Y.; Wu, L.; Cai, X.; Sun, X.; Sun, X. Photooxidative damage in retinal

pigment epithelial cells via GRP78 and the protective role of grape skin polyphenols. *Food Chem Toxicol* **74:**216-224; 2014.

[54] Chandra, J.; Samali, A.; Orrenius, S. Triggering and modulation of apoptosis by oxidative stress. *Free Radic Biol Med* **29:**323-333; 2000.

[55] Trovato Salinaro, A.; Cornelius, C.; Koverech, G.; Koverech, A.; Scuto, M.; Lodato, F.; Fronte, V.; Muccilli, V.; Reibaldi, M.; Longo, A.; Uva, M. G.; Calabrese, V. Cellular stress response, redox status, and vitagenes in glaucoma: a systemic oxidant disorder linked to Alzheimer's disease. *Front Pharmacol* **5:**129; 2014.

[56] Susin, S. A.; Lorenzo, H. K.; Zamzami, N.; Marzo, I.; Snow, B. E.; Brothers, G. M.; Mangion, J.; Jacotot, E.; Costantini, P.; Loeffler, M.; Larochette, N.; Goodlett, D. R.; Aebersold, R.; Siderovski, D. P.; Penninger, J. M.; Kroemer, G. Molecular characterization of mitochondrial apoptosis-inducing factor. *Nature* **397:**441-446; 1999.

[57] Luthert, P. J.; Chong, N. H. Photoreceptor rescue. *Eye (Lond)* **12 (Pt 3b):**591-596; 1998.

[58] Wenzel, A.; Grimm, C.; Samardzija, M.; Reme, C. E. Molecular mechanisms of light-induced photoreceptor apoptosis and neuroprotection for retinal degeneration. *Prog Retin Eye Res* **24:**275-306; 2005.

[59] Hafezi, F.; Steinbach, J. P.; Marti, A.; Munz, K.; Wang, Z. Q.; Wagner, E. F.; Aguzzi, A.; Reme, C. E. The absence of c-fos prevents light-induced apoptotic cell death of photoreceptors in retinal degeneration in vivo. *Nat Med* **3:**346-349; 1997.

[60] Kasote, D. M.; Hegde, M. V.; Katyare, S. S. Mitochondrial dysfunction in psychiatric and neurological diseases: cause(s), consequence(s), and implications of antioxidant therapy. *Biofactors* **39:**392-406; 2013.

Figure Legends

Fig. 1 RSV protects 661W cells against GD or light exposure-induced injuries. A, Hormetic effects of RSV indicate by the dose-response curve of RSV in treated 661W cells. After 16 h of treatment, RSV increased 661W cell viability at low concentrations but decreased viability at concentrations ≥ 10 μM (IC50: 209.6 μM). Values are expressed as the mean ± SEM (n = 6). **B and C,** Impedance measurements allow real-time monitoring of the viability of 661W cells under GD or light exposure in the absence or presence of varying RSV concentrations. The normalized cell index on the Y-axis is a measure of cell viability and the X-axis is time (in hour). The first black arrow represents the start of GD/light exposure and the application of RSV, and the second black arrow indicates the end of the experiment. DMEM is the control group in both B and C. **D and E,** 661W cells were treated with various concentrations of RSV (10, 50, 100 μM) under GD or light exposure (Lt) for the indicated times. Cell death was evaluated by PI/Hoechst staining. PI-positive cells can be identified by purple fluorescence and all nuclei were counterstained with Hoechst dye (blue fluorescence). Scale bar = 100 μm. **F and G,** The percentage of dead cells was calculated as PI-positive cells/Hoechst stained cells times 100. Data are shown as mean ± SEM (n = 5, $***P < 0.001$ compared to the control group, $###P < 0.001$ compared to the vehicle group.)

Fig. 2 RSV attenuated GD or light exposure-induced intracellular ROS generation. A and B, 661W cells were treated with various concentrations of RSV (10, 50, 100 μM) under GD or light exposure for the indicated times. Intracellular

ROS was measured with a DCFH-DA fluorescent probe identified by green fluorescence. Scale bar = 50 μm **C and D,** Fluorescence intensities were measured and statistically analyzed. The results are presented as the mean ± SEM (n = 5, ∗∗∗P < 0.001 compared to the control group, ###P < 0.001 compared to the vehicle group). **E,** The GSH/GSSG ratio was measured by the GSH and GSSG Assay Kit, and the results are presented as the mean ± SEM (n = 5, ∗∗∗P < 0.001 compared to the control group, ###P < 0.001 compared to the GD group, and &&& P < 0.001 compared to the light-exposure group). **F,** 661W cells were cultured in either normal DMEM, glucose-free medium, under light exposure (Lt) or in the presence of 100 μM RSV for indicated time periods. Levels of HO-1 in the whole cell lysates were determined by western blotting. β-actin was used as the loading control. **G and H,** Protein band intensity of the western blots were determined by optical density measurements and the ratio of HO-1/actin was calculated. The results are presented as the mean ± SEM (n = 3, ∗∗∗P < 0.01 compared to vehicle group).

Fig. 3 RSV maintains mitochondrial function. A, 661W cells were treated with 100 μM RSV under GD or light exposure (Lt) for the indicated times. Mitochondrial morphology was labeled with Mito Tracker Green and visualized using a confocal laser scanning microscope. The normal, elongated shape of mitochondria is altered in GD or Lt conditions but restored after RSV treatment. Scale bar = 20 μm. **B and C,** 661W cells were treated with various concentrations of RSV (10, 50, 100 μM) under GD or Lt for the indicated times. The mitochondrial membrane potential was analyzed by JC-1 fluorescent staining. The mitochondria with normal Δψm were

stained with red punctuated fluorescence (JC-1 positive), but mitochondria with depolarized Δψm were stained with green fluorescence. Scale bar = 20 μm. **D and E,** Fluorescence intensities were measured and relative fluorescence was statistically analyzed. Data are shown as mean ± SEM (n = 5, ∗∗∗P < 0.001 compared to the control group, ###P < 0.001 compared to the vehicle group)

Fig. 4 RSV activates Sirt-1 to protect 661W cells. A and C, 661W cells were treated with 100 μM RSV under GD or light exposure (Lt), in the absence or presence of the Sirt-1 inhibitor (180 μM Ex-527; Ex) for the indicated times. Cell death was evaluated by PI (purple) and Hoechst (blue) staining. Scale bar = 100 μm. **B and D,** The quantitative analysis of cell death, where the percentage of dead cells was calculated as PI-positive cells/Hoechst stained cells times 100. Data are shown as mean ± SEM (n = 4, ###P < 0.001 compared to the control group, ***P < 0.001 compared to the vehicle group). **E,** 661W cells were cultured either in normal DMEM, glucose-free medium [60], or under light exposure (Lt), as well as in the presence of 100 μM RSV for indicated time periods. Levels of Sirt1 in the whole cell lysates were determined by western blotting, with β-actin as the loading control. **F and G,** Protein band intensity was determined by optical density measurements and the ratio of Sirt1/actin was calculated. The results are presented as mean ± SEM (n = 3, ∗∗P < 0.01, ∗∗∗P < 0.001 compared to the vehicle group). **H,** The activity of Sirt1 in nuclear extracts was measured by the SIRT Activity Assay Kit and the results presented as mean ± SEM (n = 5, ∗∗∗P < 0.001 compared to the control group, ###P < 0.001 compared to the GD group, &&&P < 0.001 compared to the light exposure group).

Fig. 5 RSV blocks GD-induced cell death via caspase-dependent pathways A, 661W cells were treated with a caspase inhibitor (z-VAD-fmk; 50 μM) under GD or light exposure for the indicated times. Cell death was evaluated by PI (purple) and Hoechst (blue) staining. Scale bar = 100 μm. **B,** The quantitative analysis of cell death, where the percentage of dead cells was calculated as PI-positive cells/Hoechst-stained cells times 100. Data are shown as mean ± SEM (n = 5, ∗∗∗P < 0.001 compared to the control group, ###P < 0.001 compared to the GD group, NS = not significant). **C,** 661W cells were cultured in normal DMEM, glucose-free medium [60], or under light exposure (Lt), as well as in the presence of 100 μM RSV for indicated time periods. Levels of caspase-3 and caspase-9 in the whole cell lysates were determined by western blotting, with β-actin as the loading control. **D and E,** Protein band intensity was determined by optical density measurements and the ratios of caspase-9/actin or caspase-3/actin were calculated. The results are presented as mean ± SEM (n = 3, ∗∗∗P < 0.001 compared to the vehicle group, NS = not significant).

Fig. 6 RSV blocks light exposure-induced cell death via PARP1-dependent pathways. A, Cell death was evaluated by PI/Hoechst staining. PI-positive cells exhibited purple fluorescence and all cells were counterstained with Hoechst dye (blue fluorescent nuclei).(a)–(d) 661W cells were cultured in normal DMEM medium for 4 days in darkness (a), light exposure (Lt) (b–d), cells transfected with negative control shRNA (NC) (c), and cells transfected with PARP1 shRNA (sh-PARP) (d). **B,** The quantitative analysis of cell death, where the dead cells was calculated as PI-positive cells/Hoechst-stained cells times 100. Data are shown as mean ± SEM (n

= 4, ∗∗∗P < 0.001 compared to the control group, &&&P < 0.001 compared to the light exposure group e, P < 0.001 compared to the NC-transfected group e). **C,** 661W cells were cultured in normal DMEM and the levels of PARP-1 in the whole-cell lysates were determined by western blotting. β-actin was used as the loading control. Protein-band intensity of the western blots was determined by optical-density measurements and the ratio of PARP-1/actin was calculated. The results are presented as the mean ± SEM (n = 3, ∗∗∗P < 0.01 compared to vehicle group, NS = not significant). **D,** 661W cells were cultured in normal DMEM, glucose-free medium, or under light exposure (Lt), as well as in the presence of 100 μM RSV for indicated time periods. Levels of AIF and PARP1 in the whole cell lysates were determined by western blotting, with β-actin as the loading control. **E and F,** Protein band intensity was determined by optical density measurements and the ratios of AIF/actin or PARP1/actin are presented as the mean ± SEM (n = 3, ∗P < 0.05, ∗∗∗P < 0.001 compared to the vehicle group, NS = not significant).

Fig. 7 RSV inhibits light exposure-induced retinal dysfunction and ONL thinning *in vivo*. A and C, Representative ERG a- and b-wave responses while assessing retinal function after light exposure, in the presence or absence of RSV. Within each graph, the top trace is the response from the right eye (RE; green) and the bottom trace is the response from the left eye (LE; blue). **B and D,** Quantification of the amplitude of a-wave and b-wave under the different conditions (n = 3, *P < 0.01, NS = not significant). **E,** Representative images of H&E staining of retinal sections to assess retinal morphology after light exposure and RSV treatment. The outer nuclear

layer (ONL) is labeled in each image. **F,** Quantification of ONL thickness presented as the mean ± SEM (n = 3, $*P < 0.05$, $***P < 0.001$ compared to the vehicle group). **G,** Retinal tissue from mice raised under normal conditions (normal), vehicle-treated mice that underwent light exposure, and RSV-treated mice that underwent light exposure were analyzed for levels of AIF and PARP-1 by western blot. β-actin was used as the loading control. **H,** Protein band intensity was determined by optical density measurements and the ratios of AIF/actin or PARP-1/actin were calculated. The results are presented as mean ± SEM (n = 3, $***P < 0.001$ compared to the vehicle group, ### $P < 0.001$).

Fig. 8 A schematic diagram of the mechanism of RSV's protective effect. After GD or light exposure of photoreceptors, different mitochondria-mediated pathways are activated and lead to cell death. RSV treatment of GD- or light-exposed cells results in the activation of Sirt-1 and HO-1, as well as a decrease in ROS production and mitochondrial membrane potential. This effectively blocks the cell-death pathways, which in glucose-deprived cells is a caspase-dependent pathway and in light-exposed cells is a PARP-dependent pathway.

Highlights

1. GD and light exposure cause oxidative stress and lead to mitochondrial dysfunction.
2. GD induces caspase-dependent cell death, while light exposure induces PARP-dependent cell death.
3. Resveratrol exhibits neuroprotection by activating Sirt1.
4. Resveratrol protects the retina from light injury by blocking the PARP-AIF pathway.